Supporting Information

for

MOF-derived Fe-doped δ-MnO_2 nanoflowers as oxidase mimics: Chromogenic sensing of Hg(II) and hydroquinone in aqueous media

Udisha Duhan,[a] Arnab Pan,[b] Ritesh Dubey,[a] Samar Layek,[*,c] Sushil Kumar[*,a] and Tapas Goswami[*,a]

Ms. Udisha Duhan, Dr. Ritesh Dubey, Dr. Sushil Kumar, Dr. Tapas Goswami,
[a] Department of Chemistry, School of Engineering, UPES Dehradun, Energy Acres Building, Dehradun, 248007, Uttarakhand, India.
E-mail: sushil.k@ddn.upes.ac.in; tgoswami@ddn.upes.ac.in
Mr. Arnab Pan,
[b] Light Stock Processing Division, CSIR – Indian Institute of Petroleum, Dehradun- 248005, Uttarakhand, India.
Dr. Samar Layek
[c] Department of Physics, Applied Sciences Cluster, UPES Dehradun, Energy Acres Building, Dehradun- 248007, Uttarakhand, India.

Materials and Methods

All the chemicals were of analytical grade and used without further purification. Manganese acetate, ferric chloride, trismic acid, sodium hypochlorite (NaOCl), mercuric chloride ($HgCl_2$) and polyvinylpyrrolidone (PVP) were procured from Sigma Aldrich. Hydroquinone (HQ), TMB, glutathione (GSH), cysteine (Cys), arginine (Arg), dopamine (Dop) and guanine (Gua) were purchased from Alfa Aesar.

Powder X-ray diffraction (PXRD) patterns have been recorded on a D8 Advance Eco-Bruker X-ray diffractometer while infrared spectra were acquired with a Shimadzu IR-Spirit FTIR spectrometer. Field-emission scanning electron microscopy (FE-SEM) images were captured using a Thermo Fisher, Nova Nano SEM 450 electron microscope. UV-Vis absorption spectra were measured with a Shimadzu UV240 spectrophotometer. Electron paramagnetic resonance (EPR) spectra were recorded using a JEOL (JES-X320) spectrometer. The morphology and composition of the samples have been analysed *via* transmission electron microscopy (TEM) on a JEOL JEM-2100 microscope. X-ray photoelectron spectroscopy (XPS) was performed using a Thermo Scientific X-ray photoelectron spectrometer to investigate the elemental composition and electronic states of the as-prepared materials. The phase formation, crystal structures and corresponding lattice parameters of MOF-derived MnO_x were analysed through Rietveld refinement using GSAS-II software package.

Preparation of 10Fe-MnO_x *via* coprecipitation method

Conventional 10Fe-MnOx was prepared using a reported coprecipitation method.[1] Typically, 2.016 g of $KMnO_4$, 0.654 g of $MnSO_4 \cdot H_2O$ were dissolved in 100 mL of deionized water. To the above mixture 10 mol% of Fe relative to Mn was added and stirred for 1 hour. Next, 2.5 mL of concentrated sulfuric acid was slowly added while stirring continued for another hour. The mixture was then heated to 80°C in a water bath and stirred vigorously for an additional hour. The resulting solution was filtered and washed with deionized water until the filtrate reached a neutral pH of 7. Finally, the product was dried in an oven at 80°C for 24 hours.

Oxidase-like activity

In order to assess the oxidase activity of MOF-derived manganese oxides, 20 mL colloidal suspension of MnO_x or **Fe-MnO_x** (1 mg/mL) was mixed with 3 mL of NaAc-HAc buffer solution (pH 4.0). Now, 20 µL of TMB (15 mM) was added, and the solution mixture was incubated at room temperature. At a regular time interval, UV-Vis absorption spectra of the reaction mixture were recorded upto 20 minutes. To optimize the assay conditions, the effects of temperature, pH, incubation time, and catalyst loading were examined. The oxidase-like activity of both undoped and Fe-doped MOF-derived samples was compared by measuring the absorbance change of TMB at 652 nm. The relative activity of the different samples was calculated using the formula: $\%\ \mathbf{relative\ activity} = \frac{A_i}{A_{max}} \times \mathbf{100}$, where A_i and A_{max} represent the target and maximum absorbance of ox-TMB at 652 nm, respectively. The steady-state kinetic experiments were performed in NaAc-Hac buffer solution (3 mL, pH 4.0) containing **10Fe-MnO_x** (20 µL, 1 mg/mL) with different concentrations of TMB (0.05-1.0 mM) under the optimized conditions. By monitoring the absorbance at 652 nm, the catalytic

behaviour was fitted with the Michaelis-Menten equation. A Lineweaver-Burk plot was fitted from the Michaelis-Menten curves. The steady-state kinetic parameters were calculated using the Lineweaver-Burk plot of the double reciprocal of the Michaelis-Menten equation: $\frac{1}{V} = \frac{K_m}{V_{max}} \frac{1}{[S]} + \frac{1}{V_{max}}$, where V represents the initial reaction velocity, V_{max} is the maximum reaction velocity, K_m denotes Michaelis-Menten constant and S refers to the TMB concentration.

Active species test

Scavenging and EPR studies have been performed to identify the catalytically active species involved in the oxidation reaction, Briefly, 5.0 mM of *p*-benzoquinone (*p*-BQ), scavengers of $O_2^{\bullet-}$, was added into the reaction mixture under optimal conditions. The oxidation of TMB was then monitored by measuring the absorbance at 652 nm. Furthermore, EPR studies were carried out with and without catalyst **10Fe-MnO$_x$** in ethanol to monitor the *in-situ* generation of ROS (reactive oxygen species). Additionally, the oxidation of TMB was conducted under aerobic and anaerobic conditions to further assess the activity of surface hydroxyls in the oxidase activity of **10Fe-MnO$_x$**.

Colorimetric sensing of HQ and Hg^{2+} ion

The HQ sensing strategy was adopted based on its antioxidant features inducing the reduction of blue colored ox-TMB to colorless TMB. In brief, **10Fe-MnO$_x$** (20 µL, 1 mg/mL) was mixed with TMB (20 µL, 15 mM) in a NaAc-Hac (pH 4.0) buffer solution. After 20 mins of incubation at room temperature, the solution stabilized to a blue color. Now, 20 µL of different concentrations (0-50 mM) of HQ were added to the above mixture. The standard calibration curve for HQ was generated with varying known concentrations of HQ. Finally, absorption spectral changes at 652 nm were monitored to detect the concentration of HQ.
The colorimetric sensing platform for Hg^{2+} detection was developed based on the formation of "S-Hg^{2+}" bonds in presence of GSH. In a typical experiment, GSH (30 mM) and different concentration of Hg^{2+} were added to the 100 mL of **10Fe-MnO$_x$** solution (0.1 mg/mL), followed by the addition of TMB solution (20 mL, 15 mM). The solution was incubated for 10 mins and the absorbance at 652 nm was measured.

HQ and Hg^{2+} sensing in real water samples

To evaluate the practical applicability of the **10Fe-MnO$_x$**/TMB assay, various real water samples (tap and river water) were collected, pre-treated, and spiked with different concentrations of Hg^{2+} ions. The samples were first centrifuged and then filtered to eliminate particulate matter. Subsequently, the stock solutions were diluted to obtain the desired concentrations of HQ and Hg^{2+}. The concentrations of HQ and Hg^{2+} were then determined colorimetrically using a calibration curve.

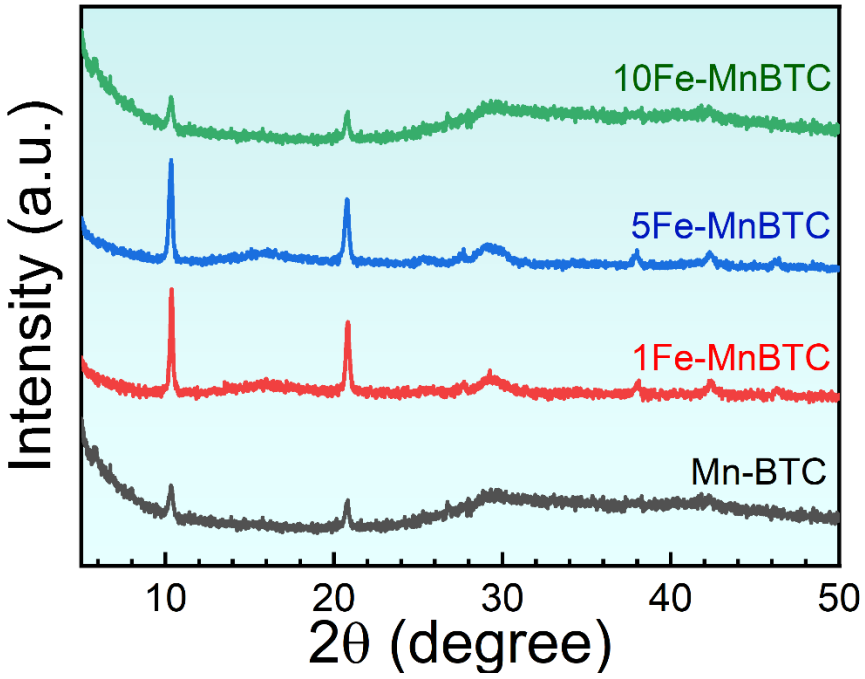

Fig. S1 PXRD spectra of MnBTC, 1Fe-MnBTC, 5Fe-MnBTC and 10Fe-MnBTC MOFs.

Table S1 Phase fraction, lattice parameters (in Å), volume (in $Å^3$) and refinement parameters for monoclinic Mn_3O_4 and tetragonal δ-MnO_2 phases extracted from the Rietveld refinement.

Sample	**Phase fraction**	**Tetragonal Mn_3O_4 (*$I4_1/amd$*)**	**Monoclinic δ-MnO_2 (*C2/m*)**	**Refinement parameters**
5Fe-MnO_x	Mn_3O_4 (~74%) δ-MnO_2 (~26%)	a = b = 5.767(4) c = 9.445(3) α = β = γ = 90º V = 314.11(4)	a = 5.148(2) b = 2.984(6) c = 7.592(3) α = γ = 90° β = 110.12(7)° V = 109.52(9)	R_{wp} = 4.22 % χ^2 = 1.376
10Fe-MnO_x	δ-MnO_2 (~100%)	-	a = 4.986(2) b = 3.111(6) c = 7.294(3) α = γ = 90º β = 100.89(3)° V = 111.12(9)	R_{wp} = 3.69 % χ^2 = 1.152

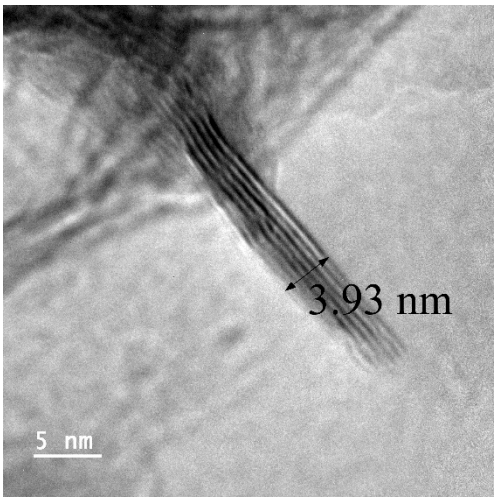

Fig. S2 HRTEM micrograph of **10Fe-MnO$_x$** used for measuring the layer thickness.

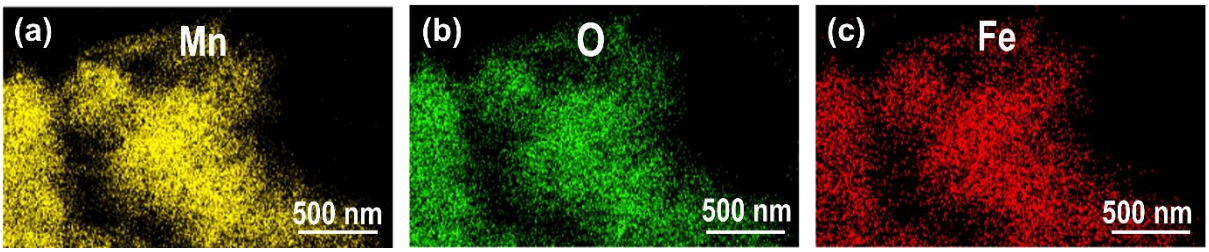

Fig. S3 EDS elemental mapping of (a) Mn, (b) O and (c) Fe in **5Fe-MnO$_x$**.

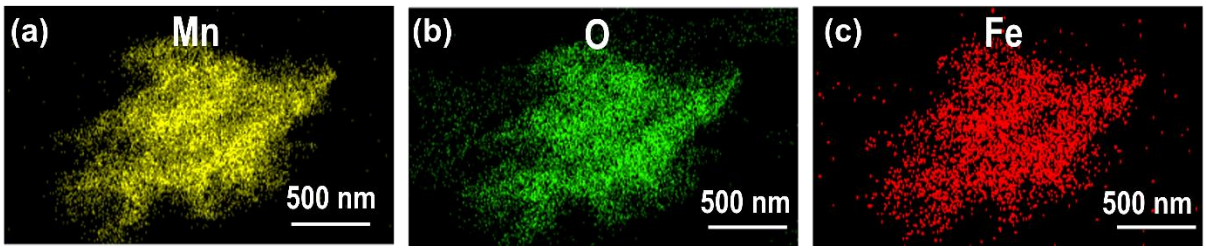

Fig. S4 The EDS elemental mapping of (a) Mn, (b) O and (c) Fe in **10Fe-MnO$_x$**.

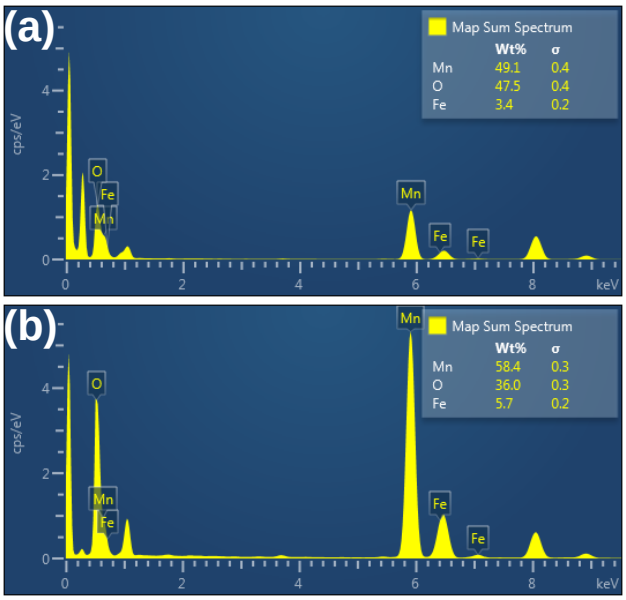

Fig. S5 The EDX spectra of (a) **5Fe-MnO$_x$** and (b) **10Fe-MnO$_x$**.

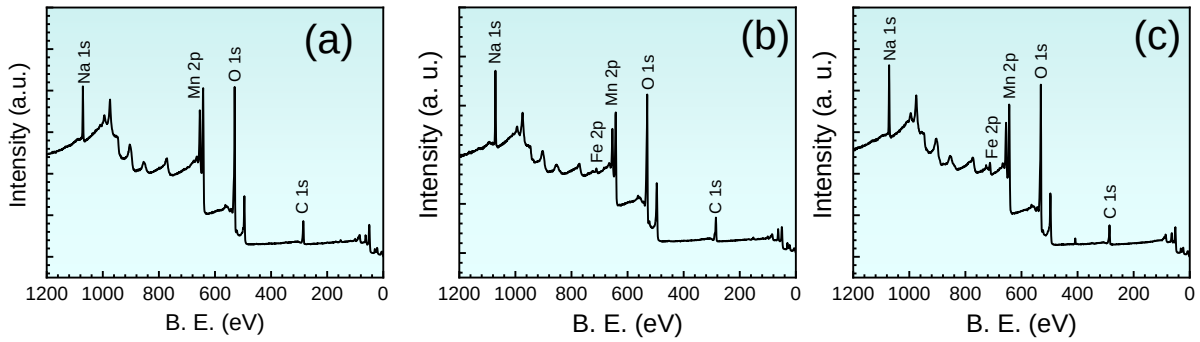

Fig. S6 XPS survey spectra of (a) MnO$_x$, (b) **5Fe-MnO$_x$** and (c) **10Fe-MnO$_x$**.

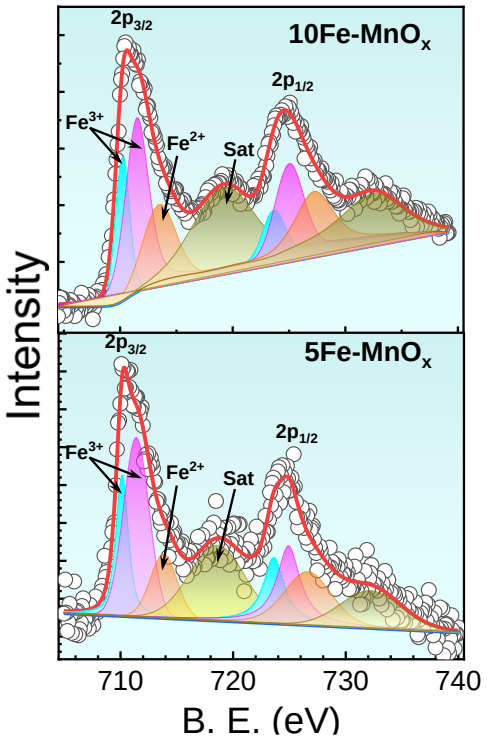

Fig. S7 XPS spectra of Fe 2p for **5Fe-MnO$_x$** and **10Fe-MnO$_x$**.

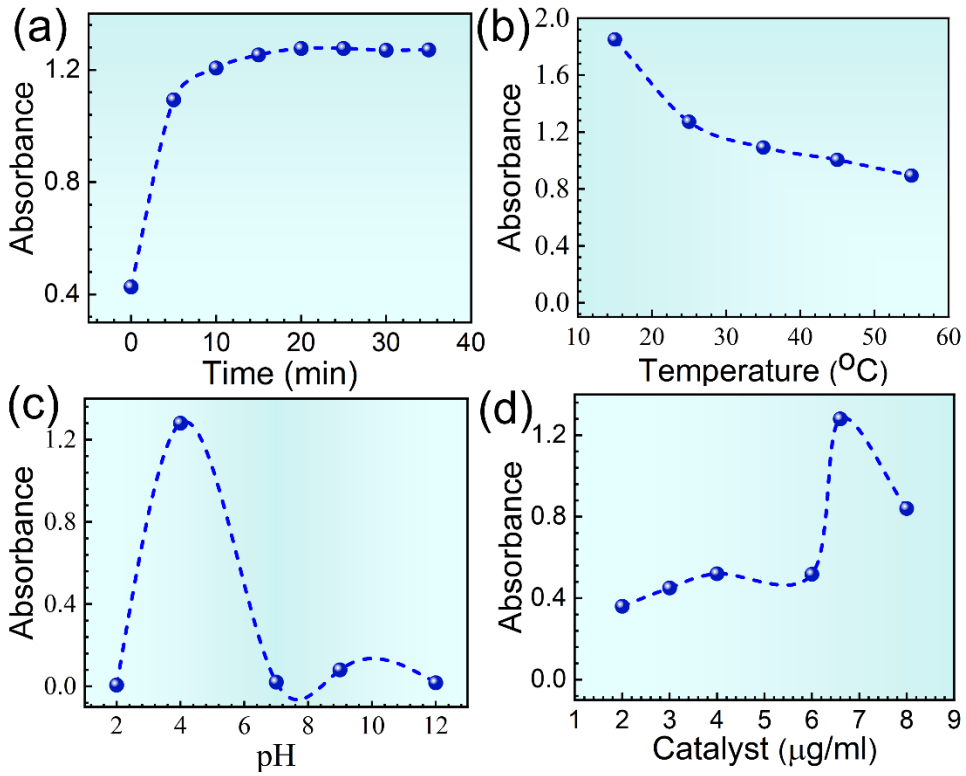

Fig. S8 Optimization of (a) time, (b) temperature, (c) pH and (d) loading of the catalyst **10Fe-MnO$_x$** for TMB oxidation reaction monitored using UV-Vis spectral changes at 652 nm.

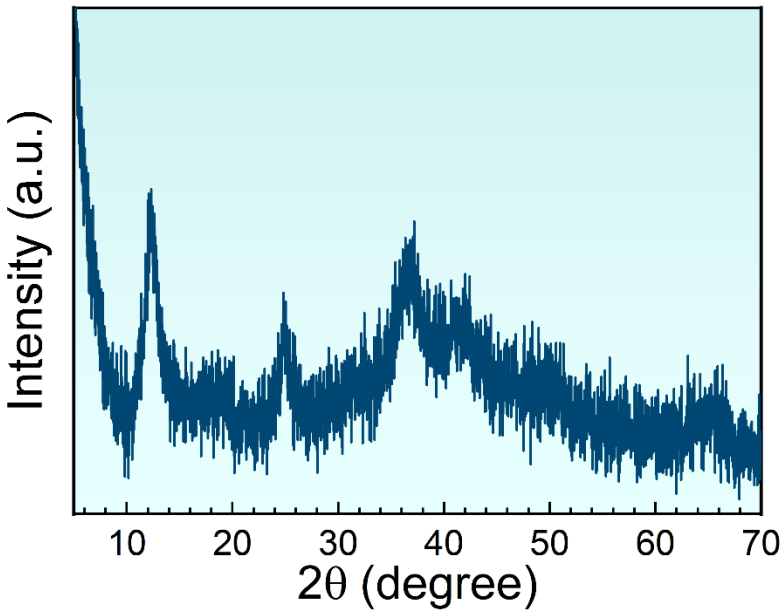

Fig. S9 PXRD pattern of 10% Fe-doped MnO_x synthesized *via* a co-precipitation method.

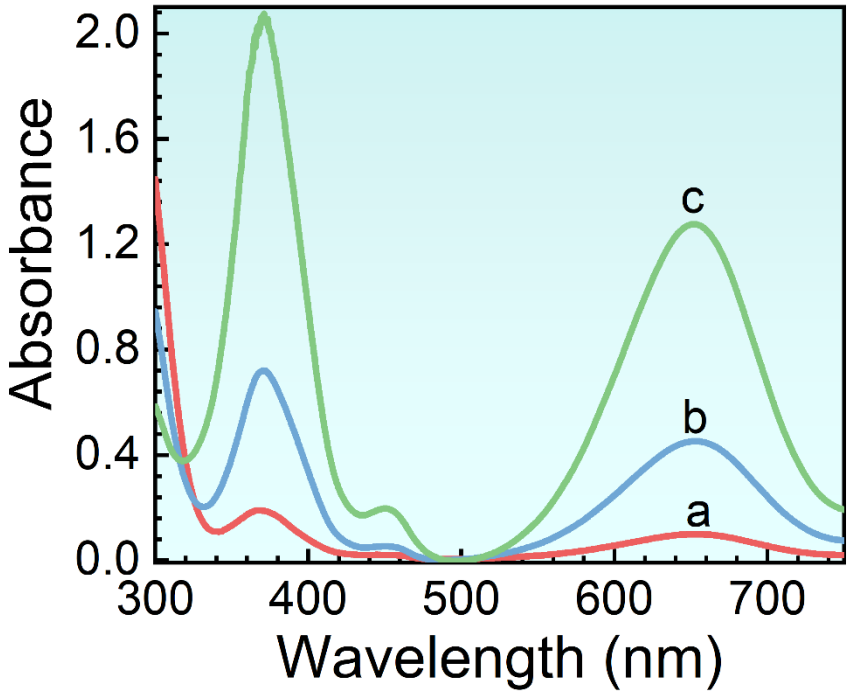

Fig. S10 Oxidase-like activity of the (a) parent MOF (10Fe-MnBTC), (b) 10% Fe-doped MnO_x synthesized *via* a co-precipitation method and (c) MOF derived **10Fe-MnO_x.**

Table S2. Comparison of K_m and V_{max} values TMB using **10Fe-MnO$_x$** with natural and other artificial enzymes.

Catalyst	**K_m(mM)**	**V_{max} (10^{-8} M)**	**Ref.**
MnO_2/GO	0.3103	2.821	[2]
Mn_3O_4	1.16	130	[3]
Mn_3O_4	1.66	3.97	[4]
MnO_2	0.246	21.9	[5]
ZIF@MnO_2	0.275	14.6	[6]
HRP	3.70	10	[7]
Catalase	4.1	-	[8]
10Fe-MnO$_x$	**0.15**	**4.03**	**This work**

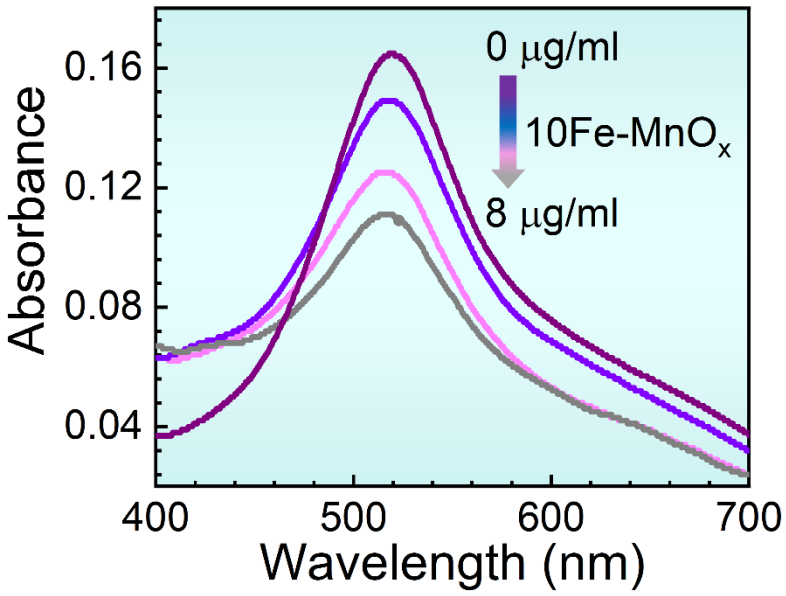

Fig. S11 (a) Change in the absorbance intensity of DPPH with different amounts of **10Fe-MnO$_x$** (0-8 μg/mL).

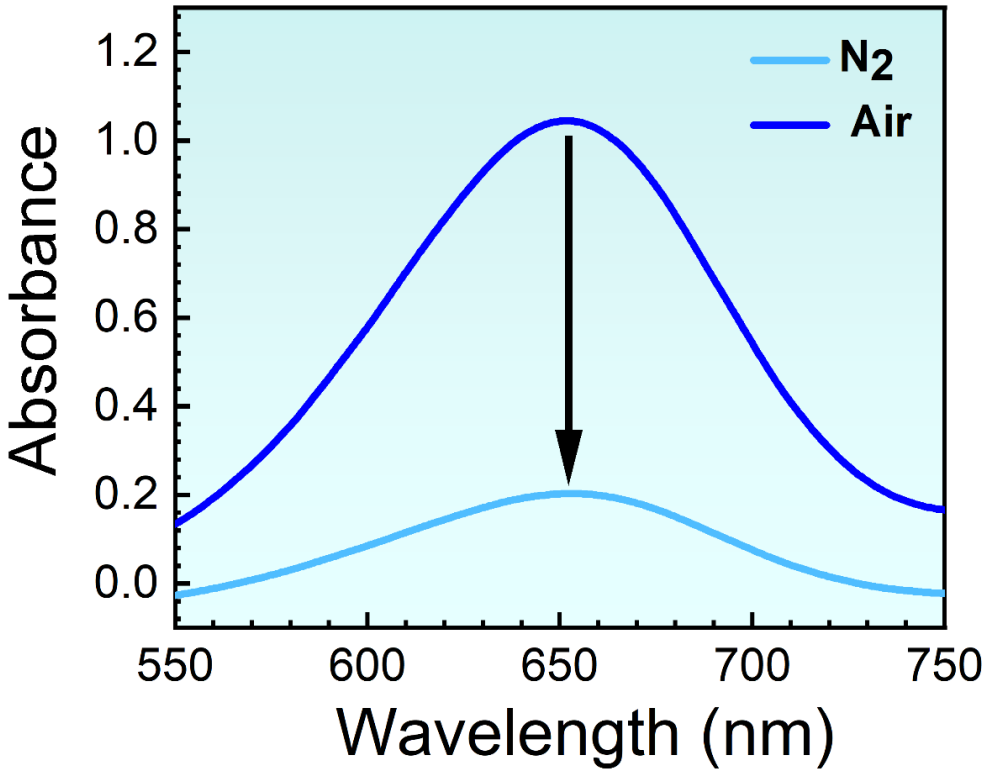

Fig. S12 UV-Vis spectra of TMB-buffer system with the addition of **10Fe-MnO$_x$** catalysts in presence of N_2 and air.

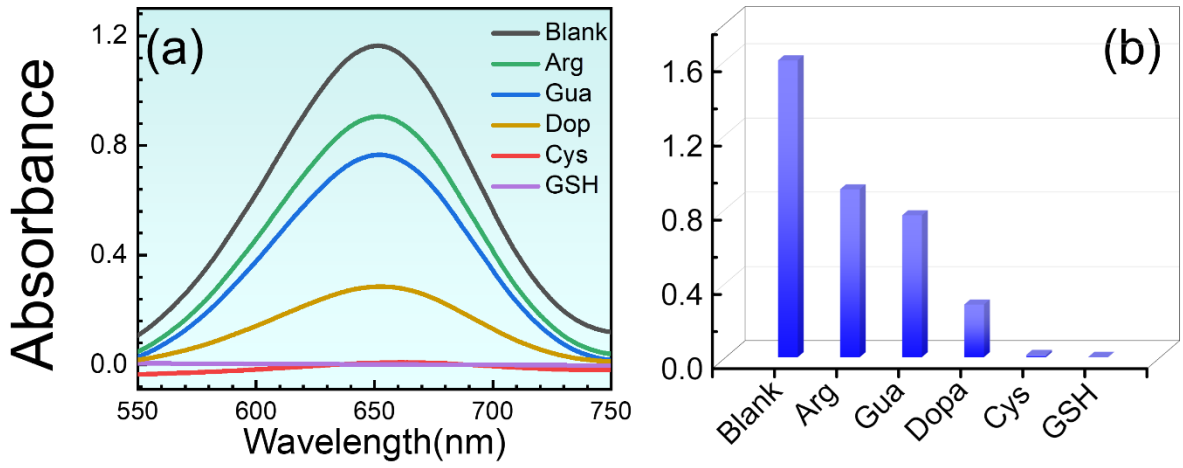

Fig. S13 (a) The absorption spectra of the **10Fe-MnO$_x$**/TMB system in the presence of different antioxidants, (b) Bar graph comparing the catalytic activities in the presence of various antioxidants using **10Fe-MnO$_x$**.

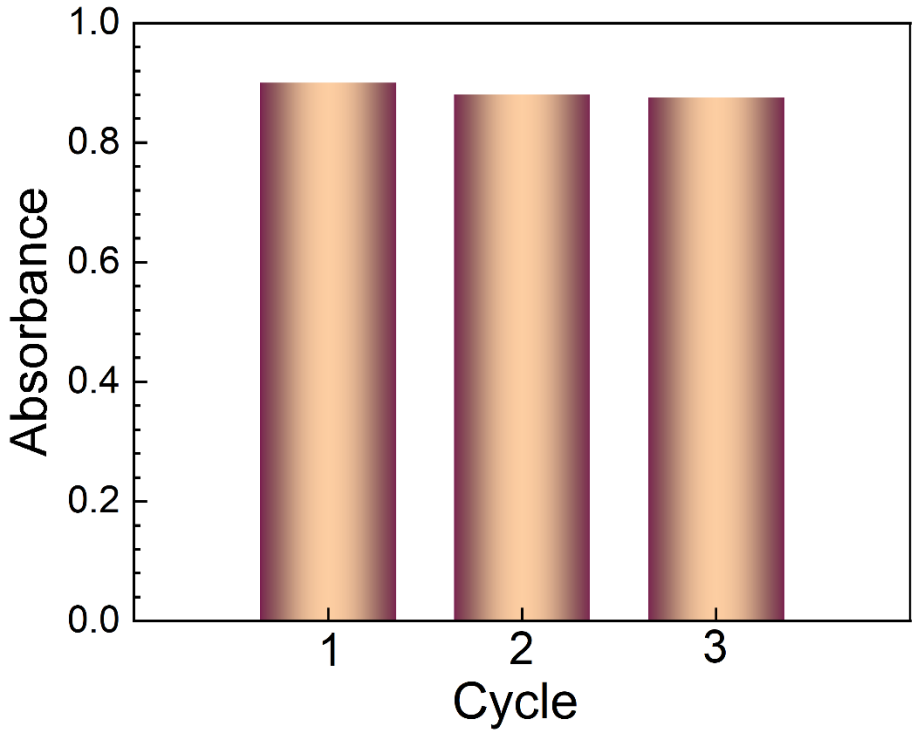

Fig. S14 Recyclability of **10Fe-MnO$_x$** for TMB oxidation reaction.

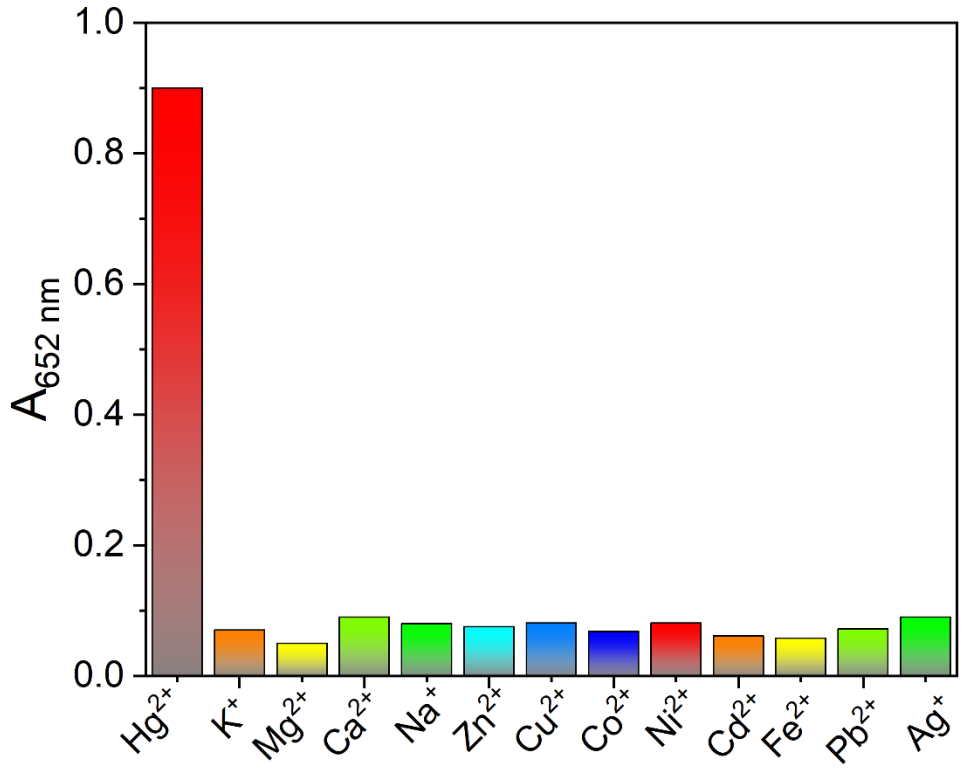

Fig. S15 The interference study for Hg^{2+} sensing in presence of various competing metal ions.

Table S3. Detection of Hg^{2+} in real samples using **10Fe-MnO$_x$**.

Real Sample	Hg^{2+} added (µM)	Hg^{2+} detected (µM)	% Recovery
Tap Water	5	4.86	97.2
	10	10.04	100.4
	20	20.05	100.2
River Water	5	5.21	104.2
	10	10.32	103.2
	20	19.67	98.35

Table S4. Detection of HQ in real samples using **10Fe-MnO$_x$**.

Real Sample	HQ added (µM)	HQ detected (µM)	% Recovery
Tap Water	5	4.94	98.8
	10	10.56	105.6
	20	19.56	97.8
River Water	5	5.06	101.2
	10	10.09	100.9
	20	19.8	99.0

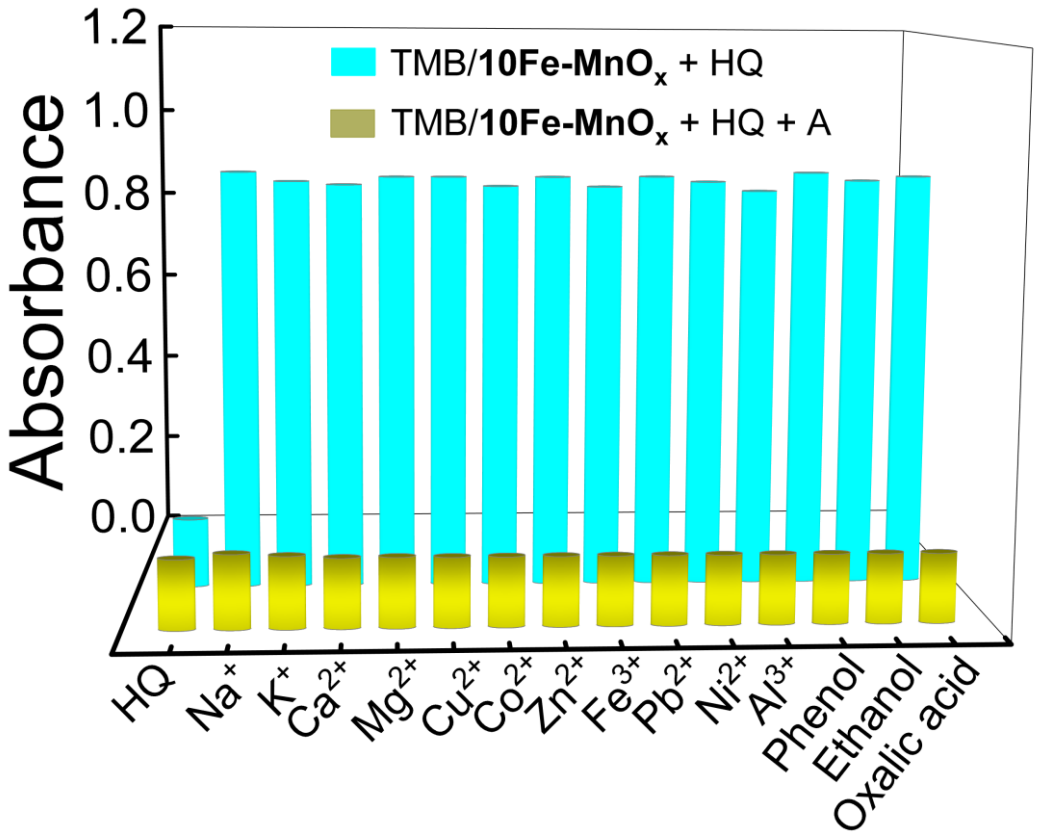

Fig. S16 Selective colorimetric detection of HQ in the presence of different interfering analytes (denoted as 'A').

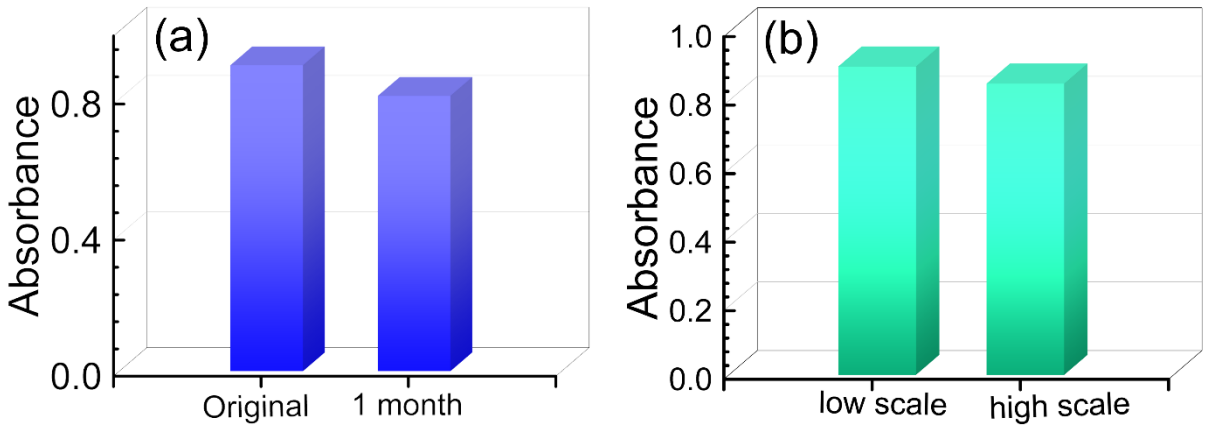

Fig. S17 Stability and scalability studies for **10Fe-MnO$_x$**.

References

1. D. Zhang, J. Dai, J. Zhang, Y. Zhang, H. Liu, Y. Xu, J. Wu and P. Li, *ACS Omega*, 2024, **9**, 18032–18045.
2. M.X. Liu, H. Zhang, S. Chen, Y.L. Yu and J.H. Wang, *Anal. Bional. Chem.*, 2021, **17**, 4451-4458.
3. Y. Wang, M. Zhao, J. Ping, B. Chen, X. Cao, Y. Huang, C. Tan, Q. Ma, S. Wu, Y. Yu, Q. Lu, J. Chen, W. Zhao, Y. Ying and Hua. Zhang, *Adv. Mater.*, 2016, **21**, 4149–4155.
4. W. Lu, J. Chen, L. Kong, F. Zhu, Z. Feng and J. Zhan, *Sens. Actuators B: Chem.*, 2021, **333**, 129560.
5. N. Liang, X. Ge, Y. Zhao, L. Xia, Z.L. Song, R.M. Kong and F. Qu, *J.Hazard. Mater.*, 2023, **454**, 131455.
6. L. Gao, J. Zhuang, L. Nie, J. Zhang, Y. Zhang, N. Gu, T. Wang, J. Feng, D. Yang, S. Perrett and X. Yan, *Nat. Nanotechnol.,* 2007, **2**, 577–583.
7. M. Christwardana, Y. Chung and Y. Kwon, *Nanoscale.*, 2017, **9**, 1993.
8. H. A. Rafiee-Pour, M. Nejadhosseinian, M. Firouzi and S. Masoum, *New J. Chem.*, 2019, **43**, 593-600.